- 1 Formation of secondary organic aerosol from nitrate radical oxidation of phenolic VOCs:
- 2 Implications for nitration mechanisms and brown carbon formation
- 3 Raphael J. Mayorga, Zixu Zhao, Haofei Zhang\*
- 4 Department of Chemistry, University of California, Riverside, California 92521, USA
- 5 \*Corresponding Author.
- 6 E-mail address: <u>haofei.zhang@ucr.edu</u> (H. Zhang).

8

9

10

11

12

13

14

15

16

17

18

19

20

21

22

23

Abstract: Volatile phenolic derivatives are substantially emitted from biomass burning and produced from photochemistry of atmospheric aromatic volatile organic compounds (VOCs). Oxidation of phenolic VOCs at night by nitrate radicals (NO<sub>3</sub>·) may represent a significant source of secondary organic aerosols (SOA) and brown carbon (BrC) formation in the atmosphere. In this study, NO<sub>3</sub>· oxidation of five phenolic derivatives, including phenol, catechol, 3-methylcatechol, 4-methylcatechol and guaiacol are investigated in laboratory experiments. The SOA constituents from the NO<sub>3</sub>· oxidation were analyzed using electrospray ionization ion mobility spectrometry time-of-flight mass spectrometry, which allows for characterization and identification of isomers in the oxidation products. Through these analyses, several classes of nitro-containing products in addition to the well-known nitrophenol compounds were observed, including: (1) the nitrophenol type of products with additional hydroxyl functional groups; (2) non-aromatic/ring-opening nitroproducts with lower double bond equivalence; (3) phenol and catechol products from the C<sub>7</sub> phenolic VOCs with carbon-containing substitutions; and (4) nitrated diphenyl ether dimers. The present work indicates that new products from previously unrecognized pathways are formed during NO<sub>3</sub>· oxidation of phenolic VOCs and may contribute an important portion of the SOA. Some of these products were also observed in ambient aerosols during biomass burning. We

- suggest that the ubiquity of the nitrophenol type of products in the SOA derived from phenolic  $VOC + NO_3$  are responsible for the strong light absorption measured in this study. Therefore,
- 26 elucidation of these pathways will be critical for understanding the nighttime oxidation and BrC
- 27 formation mechanisms.
- 28 Key words: biomass burning, light absorption, nighttime oxidation, ion mobility spectrometry,
- 29 nitrophenols

#### 1. Introduction

Wildfires are becoming increasingly severe globally and biomass burning events have been shown to strongly influence tropospheric chemistry, the climate, and human health (Crutzen and Andreae, 1990, Pope and Dockery, 2006). Namely, volatile organic compounds (VOCs) and nitrogen oxides ( $NO_x$ ) emitted from biomass burning undergo various oxidation reactions in the troposphere, substantially impacting the tropospheric ozone ( $O_3$ ) budget (Arnold et al. 2015). Further, secondary organic aerosols (SOA) from these oxidation reactions can affect the Earth's radiative balance by scattering and absorbing solar radiation in the troposphere (Hobbs et al., 1997). Phenolic derivatives have been shown to make up an important portion of the VOC emissions during biomass burning events (Hatch et al., 2015). They are also key intermediates from photooxidation of aromatic hydrocarbons (also abundant from biomass burning emissions) in the atmosphere (Bloss et al. 2005). The major phenolic VOCs have total emission factors ranging from 0.10 to 0.64 g kg<sup>-1</sup> from the combustion of fuels native to the western United States (Hatch et al. 2015; Fine, Cass, and Simoneit, 2004; Oros and Simoneit, 2001). Moreover, their SOA formation potential is among the highest due to their relatively large SOA yields (Hatch et al., 2017). These

SOA are often found to be light absorbing (i.e., forming brown carbon, BrC), which further enhance their climate impacts (Lin et al. 2018, 2017, 2015).

45

46

47

48

49

50

51

52

53

54

55

56

57

58

59

60

61

62

63

64

65

66

67

There have been extensive studies on the oxidation of phenolic VOCs and most of them have focused on hydroxyl radical (·OH) oxidation (Finewax et al. 2019, 2018; Kroflič et al. 2015; Lauraguais et al. 2016; Nakao et al. 2011; Pang et al. 2019; Pereira et al. 2015; Schwantes et al. 2017; Vidović et al. 2020). In these studies, phenolic VOCs such as phenol, catechol, 3methylcatechol (3MC), 4-methylcatechol (4MC), and guaiacol have been shown to produce SOA in high yields ranging from 25-145% from OH-initiated chemistry (Coeur-Tourneur et al. 2010; Finewax et al. 2018; Lauraguais et al. 2014; Nakao et al. 2011; Pereira et al. 2015; Schwantes et al. 2017; Vidović et al. 2020; Yee et al. 2013). The OH-oxidation of phenolic VOCs in the presence of nitrogen oxides (NO<sub>x</sub>) were also found to produce large amounts of BrC, due to the substantial formation of nitrophenol products (Bluvshtein et al. 2017; Fleming et al. 2020; Lin et al. 2018, 2017, 2015). These products, such as nitrophenols and nitrocatechols, have been reported from laboratory studies and field measurements (Bluvshtein et al. 2017; Finewax et al. 2018; Fleming et al. 2020; Lin et al. 2018, 2017, 2015). The phenolic VOCs could also be oxidized by nitrate radicals (NO<sub>3</sub>·) which, however, has been understudied. The NO<sub>3</sub>· oxidation could be an important reaction pathway of phenolic VOCs during nighttime, relevant to both biomass burning events and urban atmosphere (Rollins et al. 2012). BrC formation has also been recently reported during NO<sub>3</sub>· oxidation of tar aerosols from wood pyrolysis which largely contain phenolic compounds (Li et al. 2020a). Despite their significance, the understanding of NO<sub>3</sub>· oxidation mechanisms of individual phenolic VOCs and the SOA formation in prior studies have been very limited. Often, nitro-phenolic compounds were the only major products reported in the SOA composition (Bolzacchini et al. 2001; Finewax et al. 2018; Frka et al. 2016; Kitanovski et al. 2014;

Vidović et al. 2020, 2018; Yuan et al. 2016). Other products such as those with additional functional groups and oligomers have not been systematically examined, despite that such low-volatility compounds could be important SOA constituents under ambient conditions. It is unclear whether and to what extent these types of products form during NO<sub>3</sub>· oxidation of phenolic VOCs.

The major SOA constituents of these reactions and the underlying mechanisms remain a challenge to uncover, largely due to the limitations in detection and identification of the particlephase products. Previously, a variety of analytical techniques have been implemented to characterize the phenolic VOC-derived SOA such as gas chromatography mass spectrometry (GC-MS), liquid chromatography mass spectrometry (LC-MS), chemical ionization mass spectrometry (CIMS), Fourier transform infrared spectroscopy (FTIR), and UV-Vis diode array detectors (Bolzacchini et al. 2001; Finewax et al. 2018; Frka et al. 2016; Kitanovski et al. 2014; Kroflič et al. 2015; Li et al. 2020a; Vidović et al. 2018; Yuan et al. 2016; Zaytsev et al. 2019). However, most of the instruments listed are incapable of unambiguously characterizing the SOA constituents, especially on the isomer level. In this study, we performed NO<sub>3</sub>· oxidation experiments in a continuous flow stirred tank reactor (CFSTR) of five phenolic VOCs, including phenol, catechol, 3MC, 4MC, and guaiacol (structures shown in **Figure 1**). We use electrospray ionization (ESI) coupled to an ion mobility spectrometry time-of-flight mass spectrometer (IMS-TOF) for offline analysis of the SOA from these experiments. The IMS-TOF allows for separation, characterization, and sometimes, identification of structural isomers. Additionally, a UV-Vis spectrometer is utilized for analysis of the light absorption of the SOA materials. With these analytical instruments, we comprehensively identify the major products from these reactions and the underlying mechanisms as well as characterize their optical properties.

68

69

70

71

72

73

74

75

76

77

78

79

80

81

82

83

84

85

86

87

88

**Figure 1.** Chemical structures of the phenolic derivatives under study.

# 2. Experimental methods

# 2.1. Chemicals and reagents

The chemicals and reagents used in the present study and their purities and suppliers are as follows: phenol (99.5%, Sigma-Aldrich), guaiacol ( $\geq$ 98%, Aldon Corporation), catechol (>99%, Tokyo Chemical Industry), 3-methylcatechol (3MC, 95%, Combi Blocks), 4-methylcatechol (4MC, 98%, Frontier Scientific), 2-nitrophenol (2NP, 98%, Tokyo Chemical Industry), 3-nitrophenol (3NP, >98%, Tokyo Chemical Industry), 4-nitrophenol (4NP, >99%, Tokyo Chemical Industry), 4-nitrocatechol (4NC, 97%, Fischer Scientific), sodium chloride (99.5%, Sigma-Aldrich), methanol (HPLC Grade Fischer Chemical), acetonitrile (HPLC Grade Fischer Chemical), and deionized (DI) water (18M $\Omega$ , purified using a Milli-Q water system). All reagents and solvents were used without further purification.

#### 2.2. Laboratory experiments

SOA was generated from oxidation of the five above-mentioned phenolic VOCs with NO<sub>3</sub>· in a custom-made CFSTR (effective volume of 250 L, stainless steel enclosure with interior coating by Teflon PFA). The CFSTR setup is illustrated in Figure 2. The total flow rate of the CFSTR was approximately 4.1 L min<sup>-1</sup> and the residence time in the CFSTR was approximately one hour. A clean air generator (Aadco Instruments, Inc., 747-30) was used to provide a constant flow of clean dry air at 2.5 L min<sup>-1</sup> and humidified air at 1.0 L min<sup>-1</sup> by bubbling dry air through DI water. The RH in the CFSTR stabilized at 35-40% for all experiments. This RH level is relevant to that observed at nighttime in the western US during summer seasons when biomass burning has a high frequency (Yuan et al. 2016). NaCl seed aerosols were generated by a constant output atomizer (TSI) and introduced into the CFSTR at ~ 0.6 L min<sup>-1</sup> without upstream drying. Nevertheless, the RH in the CFSTR is maintained below the efflorescence RH of NaCl (45 – 55%) and thus the seed aerosols were dry throughout the experiments (Gao et al. 2007), to minimize reactive uptakes of NO<sub>3</sub>· and N<sub>2</sub>O<sub>5</sub> and avoid aqueous-phase chemistry (Gershenzon et al. 1999; Phillips et al. 2016; Seisel et al. 1997; Stewart et al. 2004; Thornton et al. 2010). The size distribution and number concentration of SOA in the CFSTR were measured using a scanning electric mobility scanner (SEMS, Brechtel Inc., 2100) and a mixing condensation particle counter (MCPC, Brechtel Inc., 1720), respectively. The background particle concentrations in the CFSTR were very low (< 0.1 μm<sup>3</sup> cm<sup>-3</sup>) before the experiments started. Once seed aerosol was injected, particle volume concentration was allowed to equilibrate to approximately 30 – 40 µm<sup>3</sup> cm<sup>-3</sup> before oxidation started. The seed aerosols were used to enhance the partitioning of gas-phase semivolatile products to the particle phase rather than loss to the walls. Each phenolic VOC of interest was injected into the CFSTR a few hours before the experiments using a syringe pump (Chemyx Inc.) at pre-calculated rates to allow the concentration of the VOC in the reactor to stabilize at

106

107

108

109

110

111

112

113

114

115

116

117

118

119

120

121

122

123

124

125

126

127

approximately 100 ppb, estimated based on the law of mass conservation. Most of the VOCs (except for guaiacol) investigated are solid at room temperature and hence were dissolved in methanol before being added into the syringe. The methanol concentrations in the CFSTR were estimated to be ~ 4 ppm. It was not expected to be involved in the oxidation chemistry, except to scavenge the negligible amount of produced ·OH. NO<sub>3</sub>· was produced by reacting O<sub>3</sub> with nitrogen dioxide (NO<sub>2</sub>) in the CFSTR. O<sub>3</sub> was generated by passing O<sub>2</sub> gas through an ozone generator (Ozone solution Inc.) at  $\sim 500 - 620$  ppb. NO<sub>2</sub> was supplied directly from a gas cylinder of NO<sub>2</sub> (20 ppm in  $N_2$ , Airgas Inc.) at 50 cm<sup>3</sup> min<sup>-1</sup>, indicative of an injection concentration of ~250 ppb. The concentrations of O<sub>3</sub> and NO<sub>2</sub> were measured using a 49C O<sub>3</sub> (Thermo Environmental Instruments) and a 42C NO-NO<sub>2</sub>-NO<sub>x</sub> analyzer (Thermo Environmental Instruments), respectively (Zhao et al. 2019a). We apply the injection rates of VOCs, O<sub>3</sub>, and NO<sub>2</sub>, as well as the measured steady-state concentrations of O<sub>3</sub> and NO<sub>x</sub> in a MCM-based kinetic model to estimate the concentrations of VOCs and NO<sub>3</sub>· under steady state (Bloss et al. 2005). Once the formed SOA,  $O_3$  and  $NO_x$  concentrations approximately reached steady state, sample collection was commenced using a sequential spot sampler (Aerosol Devices Inc.) at 1.6 L min<sup>-1</sup> for 2 hours. After collection, the sample was immediately extracted into 60 µL acetonitrile with 0.1 mM NaCl for analysis by the IMS-TOF. At this time, another sample collection was begun using the spot sampler again at 1.6 L min<sup>-1</sup> for another 2 hours. This sample was immediately extracted into 500 μL methanol for analysis with a UV-Vis spectrophotometer.

129

130

131

132

133

134

135

136

137

138

139

140

141

142

143

144

145

146

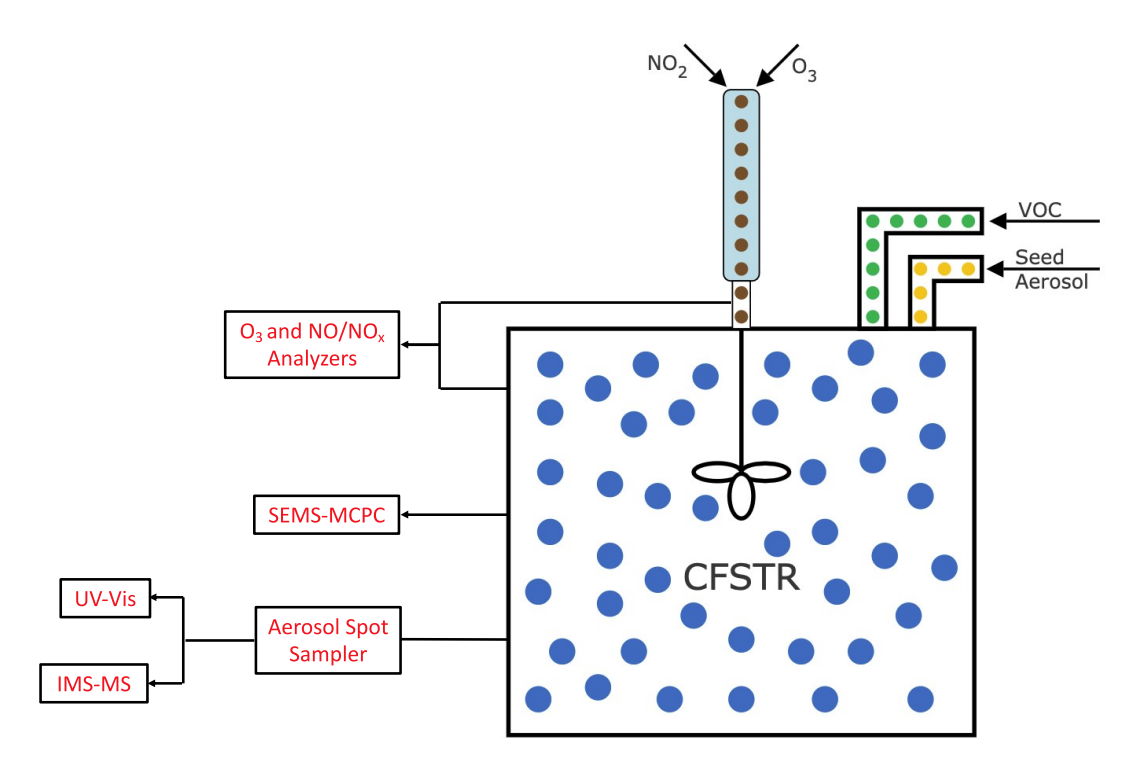


**Figure 2**. A diagram of the experimental setup is shown on the right which includes the CFSTR, VOC, O<sub>3</sub>, NO<sub>2</sub>, and seed aerosol injection lines. On the left, corresponding arrows are drawn to the analytical tools which were implemented in this study.

#### 2.3. *IMS-TOF*

Following extraction of the samples into 60  $\mu$ L acetonitrile with 0.1 mM NaCl, the samples were immediately analyzed using the IMS-TOF instrument (Tofwerk Inc. and Aerodyne Research Inc.) with ESI in the negative ion mode. The ACN-NaCl combined solvent was tested to lead to the best ionization efficiency using various chemical standards (Zhao et al. 2020, 2019a, 2019b). A detailed description of the instrument has been provided in our recent publications (Zhao et al. 2020, 2019a, 2019b). The organic concentration in the extracts ranged from ~50 ng  $\mu$ L<sup>-1</sup> (phenol SOA) to ~200 ng  $\mu$ L<sup>-1</sup> (catechol SOA). To further validate the atmospheric relevance of the products characterized from the laboratory experiments, a PM<sub>1</sub> aerosol sample collected from Centreville, AL, during the 2013 Southern Oxidant and Aerosol Study (SOAS) field campaign was

analyzed using the IMS-TOF. This ambient sample was collected during the major biomass burning event on June 4<sup>th</sup>, 2013 from ~4 am to ~4 pm (Zhang et al. 2018). Thus, the composition in this aerosol sample could represent a combination of nighttime and daytime processing of the biomass burning emissions. This ambient aerosol sample was extracted following the procedure published previously before analysis (Zhang et al. 2011a, 2012a, 2012b). Each sample extract was introduced into the instrument using a 250 µL syringe (Hamilton) mounted on a syringe pump (KD Scientific Inc.) with a flow rate of 1 µL min<sup>-1</sup>. The samples were ionized by negative-mode ESI (-1650 V) before introduction into the drift tube. In our prior studies we reported nitrate and nitro species clustering with Cl<sup>-</sup> in (-)ESI-IMS-TOF (Zhang et al. 2019). But for nitro-phenolic species that are slightly acidic the dominant ionization scheme turned out to be [M-H]. The flow of ions was aided by a flow of N<sub>2</sub> gas at 0.8 L min<sup>-1</sup>. The drift tube was held at a constant pressure of 1000 mbar and a constant temperature of 60.0°C. The ions were met with a counterflow of N<sub>2</sub> gas at 1.2 L min<sup>-1</sup> which served to separate the ions based on their size and geometry, termed as their collisional cross-section (CCS). Based on their extent of interaction with N<sub>2</sub> gas, each ion exits the drift tube with a specific drift time (Zhao et al. 2019a). Next, the ions are focused into a pressure-vacuum interface composed of two segmented quadrupoles. Collision-induced dissociation (CID) can occur between the two segmented quadrupoles by adjusting the voltages on the ion optical elements (Zhang et al. 2019). Thus, the IMS-TOF allows for isomer-resolved characterization of the collected SOA constituents. In an effort to unambiguously identify the single nitro-products of phenol and catechol, chemical standards were run in the IMS-TOF for 2nitrophenol (2NP), 3-nitrophenol (3NP), 4-nitrophenol (4NP), and 4-nitrocatechol (4NC). The IMS-TOF instrument was operated over an m/Q range of 20-1500 Th. The average resolution of the IMS is  $(t/\Delta t) \sim 100$  and for the TOFMS  $(m/\Delta m) \sim 4000$  (Zhang et al. 2019). All post processing

164

165

166

167

168

169

170

171

172

173

174

175

176

177

178

179

180

181

182

183

184

185

was done using Tofware (version 3.2.0, Tofwerk) running with Igor Pro (WaveMetrics, OR, USA)

188 (Zhao et al. 2019a).

*2.4. UV-visible spectroscopy* 

All UV-Vis spectroscopy measurements (Agilent Inc. 8453) were operated under 293 K and 1 atm. A 500  $\mu$ L cuvette with a path length of 1.0 cm was used and all samples were run using methanol as the solvent. Three trials were run for each sample and the averaged results were reported. The data from this analysis was used to calculate the mass absorption coefficient (MAC) in m<sup>2</sup> g<sup>-1</sup> and averaged <MAC> for each sample. The equations for these MAC are shown here:

195 
$$MAC(\lambda) = \frac{A(\lambda) \times \ln{(10)}}{b \times C_m}$$

where  $A(\lambda)$  is the absorbance at the wavelength of interest, b is path length of cuvette (0.01 m) and

 $C_m$  is the concentration of SOA in g m<sup>-3</sup> (Jiang et al. 2019).

$$< MAC > = \frac{\sum_{i=1}^{n} MAC(\lambda_i)}{n}$$

The averaged MAC was calculated over the range of 290 - 700 nm and 400 - 550 nm so that our results can be compared with prior relevant studies.

#### 3. Results and discussion

3.1. SOA formation from NO<sub>3</sub>· oxidation of phenolic VOCs and general mechanisms

The experimental setup used in this study leads to SOA formation from  $NO_3$ · oxidation of phenolic VOCs under approximate steady state. **Table 1** summarizes the experimental conditions. The timeseries for total aerosol mass and oxidant concentrations ( $O_3$  and  $NO_x$ ) are shown in the **Supporting Information (SI)**, **Figure S1**. Because a direct  $NO_3$ · measurement was not available in this work, we used the MCM mechanism to provide approximate estimates of  $NO_3$ ·

concentrations based on the injected and measured  $O_3$  and  $NO_x$  (Bloss et al. 2005). In the MCM box model simulations, the injection concentrations were either measured directly (O<sub>3</sub> in the injection line) or estimated based on the law of mass conservation (for the phenolic VOCs and NO<sub>2</sub>). The MCM mechanism (detailed in the SI, Table S1) includes detailed gas-phase reactions for phenol, catechol, and 3MC, but not for 4MC and guaiacol. Thus, the initial NO<sub>3</sub>· oxidation reactions are added for 4MC (1.47  $\times$  10<sup>-10</sup> cm<sup>3</sup> molecules<sup>-1</sup> s<sup>-1</sup>) and guaiacol (2.69  $\times$  10<sup>-11</sup> cm<sup>3</sup> molecules <sup>1</sup> s <sup>-1</sup>), using the rate constants reported in previous research (**Table S2**, Lauraguais et al. 2016; Olariu et al. 2004). The products for 4MC oxidation are assumed to be the same as those for 3MC oxidation, while further reactions for guaiacol are not included due to limited information available. In addition, the loss rates of gas-phase  $NO_3$  and  $N_2O_5$  onto the Teflon wall  $(1.5 \times 10^{-3}$  $s^{-1}$  and 0, respectively) and the dry NaCl seed aerosols (5.0 × 10<sup>-3</sup>  $s^{-1}$  and 2.0 × 10<sup>-3</sup>  $s^{-1}$ , respectively) are specifically represented in the simulations, using rates reported in previous studies (Fry et al. 2014; Gershenzon et al. 1999; Stewart et al. 2004). All other gas-phase species are assumed to have wall loss rates of  $5.0 \times 10^{-5}$  s<sup>-1</sup>. The simulated O<sub>3</sub> concentrations at approximate steady state for the five experiments are generally consistent with the measurements, while the NO<sub>x</sub> concentrations were under predicted (shown in Figure S1, SI). This is likely due to the interference in  $NO_x$  measurements by other inorganic and organic nitrogen. The kinetic models suggest that the  $NO_3$  concentrations in the experiments were on the order of 0.4 - 15 ppt under steady state, as shown in **Table 1**. The much higher steady-state NO<sub>3</sub>· concentration for the phenol experiment is due to the slower reaction rate  $(3.8 \times 10^{-12} \text{ cm}^3 \text{ molecules}^{-1} \text{ s}^{-1})$ , compared to those of the other phenolic VOCs. Under the experimental conditions, the box model simulations suggest that the produced ·OH concentrations are very low ( $< 5 \times 10^5$  molecules cm<sup>-3</sup>) and the majority (> 90%) of the phenolic VOCs reacted with NO<sub>3</sub>·, rather than O<sub>3</sub> or ·OH. We should note that the MCM

209

210

211

212

213

214

215

216

217

218

219

220

221

222

223

224

225

226

227

228

229

230

NO<sub>3</sub>· oxidation mechanisms for the phenolic VOCs used here are not necessarily comprehensive and accurate; certain concentrations and rate constants were estimated because key gas-phase measurements were unavailable. Nevertheless, the goals of using these simulations were not to accurately describe the oxidation reactions, but rather to (1) demonstrate that NO<sub>3</sub>· oxidation is the main loss pathway for the phenolic VOCs; and (2) develop a basic understanding of the oxidation regimes (e.g., concentrations of NO<sub>3</sub>·, reacted amounts of VOCs, etc.). The formed SOA mass concentrations from the steady-state experiments should be interpreted differently from the typical batch-mode chamber experiments and hence are not directly comparable. This is likely due to the short reaction time (~1 hr) in the present experimental setup and we expect that the observed SOA yields are likely lower than from other chamber experiments. Further, despite of the usage of seed aerosols, the relatively small reactor volume could have caused some wall loss of the gas-phase oxidation products. In addition, the parent phenolic VOCs might also have significant wall losses due their functionality that could more substantially lead to lower SOA formation (Matsunaga and Ziemann 2010). The vapor wall loss, however, should have little influence on the molecular characterization and optical properties of the SOA constituents.

247

248

249250

251252

253

232

233

234

235

236

237

238

239

240

241

242

243

244

245

246

**Table 1.** Experimental conditions.

VOC	Injected/steady -state <sup>a</sup> [VOC] (ppb)	Injected <sup>b</sup> /steady- state [O <sub>3</sub> ] (ppb)	Injected <sup>b</sup> /steady- state [NO <sub>x</sub> ] (ppb) <sup>c</sup>	Estimated steady-state <sup>a</sup> [NO <sub>3</sub> ·] (ppt)	SOA mass concentration (µg m <sup>-3</sup> ) <sup>d</sup>	<mac> values (m<sup>2</sup> g<sup>-1</sup>) (365 nm/400-500 nm/290-700 nm)<sup>e</sup></mac>
Phenol	100/15.9	580/420	250/190	13.7	16.5	1.307/0.413/0.896
Catechol	100/17.6	450/325	250/110	0.4	65.6	3.121/0.799/1.389
3MC	100/8.5	600/415	250/125	0.6	56.8	1.981/0.553/0.974
4MC	100/8.7	600/400	250/130	0.6	40.5	1.990/0.973/1.298
Guaiacol	100/25.0	500/330	250/120	1.0	46.5	0.618/0.171/0.304

<sup>a</sup>Steady-state VOCs are estimated by the kinetic model; <sup>b</sup>injected concentrations of  $O_3$  and  $NO_x$  are based on injection rates; <sup>c</sup>the steady-state  $NO_x$  was measured by the  $NO_x$  analyzer and could include some interference from other inorganic and organic nitrogen; <sup>d</sup>a density of 1.4 g cm<sup>-3</sup> was assumed for the average density of SOA; <sup>e</sup>the 400-500 nm and 290-700 nm results are averaged values within the specific wavelength ranges.

255

256

257

258

259

260

261

262

263

264

265

266

267

268

269

270

271

272

273

274

275

276

The generalized initial gas-phase reaction scheme of NO<sub>3</sub>· oxidation of phenolic VOCs that leads to the addition of one nitro group (-NO<sub>2</sub>) to the phenolic backbone is shown in **Figure 3A**. It can likely be applied to the other phenolic VOCs studied here with slight adjustments (Bolzacchini et al. 2001; Kroflič et al. 2015; Vidović et al. 2018). Presented in Figure 3B is a more comprehensive mechanism showing the gas-phase formation pathways of the main products from the NO<sub>3</sub>· oxidation of phenol including the nitro- and dinitro-phenols as well as a variety of their dimer products, which likely undergo gas-particle partitioning and were measured in the particle phase. The other studied phenolic VOCs all likely undergo similar mechanisms to form monomeric and dimeric products with 1-3 nitro groups. Some possible exceptions are discussed in later sections. The mechanism shown here, however, only presents the formation of nitro-phenolic products. Whether and how other types of products (e.g., additional functional groups on the aromatic ring) could be formed remains unclear. In Figure 3A, the highlighted portion in green represents a phenyl radical intermediate whose stability determines the likelihood of isomeric ratios of the products. It should be noted that the type and number of substitution groups occupied on the initial aromatic ring likely govern the intermediate's stability, and hence the isomer preference and diversity. For example, prior studies suggest that 2NP and 4NC are the dominant products from NO<sub>3</sub>· oxidation of phenol and catechol, respectively, in the absence of O<sub>3</sub> (Bolzacchini et al. 2001; Finewax et al. 2018). However, Bolzacchini et al. reported that the presence of O<sub>3</sub> could affect the intermediate's stability during the phenol NO<sub>3</sub>· oxidation and change the nitrophenol isomers' distribution (i.e., leading to the formation of 4NP). How the relevant isomers are distributed in the real atmosphere where O<sub>3</sub> is usually present in comparison to laboratory studies have not been demonstrated.

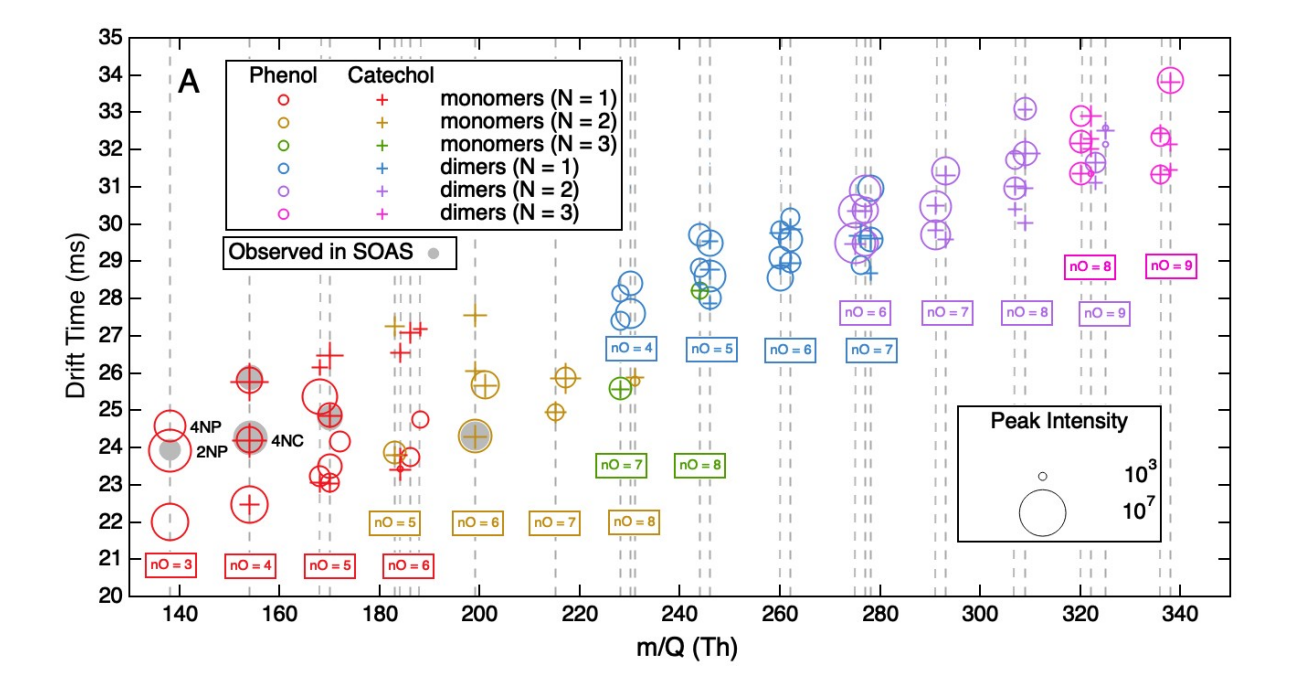
**Figure 3.** (A) General mechanism for the NO<sub>3</sub>· oxidation of phenolic VOCs leading to the nitrophenol type of products. The various R groups represent a variety of functional groups including -H, -OH, -OCH<sub>3</sub>, -CH<sub>3</sub>. The structure highlighted in green represents a key phenyl radical intermediate in the mechanism. (B) General mechanism for the NO<sub>3</sub>· oxidation of phenol to form single-nitro phenols (orange), dinitrophenol (red), single-nitro dimers (pink), dinitro dimers (blue) and a tri-nitro dimer (purple).

3.2. Characterization of the SOA constituents from NO<sub>3</sub>· oxidation of the phenolic VOCs

The IMS is capable of separating isomers based on their CCS and the TOF allows for accurate molecular formula characterization of the products. The capability of the instrument to provide fragment mass spectra further facilitates identification of functional groups in the products

and investigation of fragmentation patterns. Therefore, detailed analysis of molecular and structural information of the phenolic VOCs  $NO_3$ · oxidation products under study are possible. **Figure 4A** presents a two-dimensional plot of the drift time vs. m/Q for all of the products observed from the  $NO_3$ · oxidation of phenol and catechol; **Figure 4B** presents the same type of plot for the products of the  $NO_3$ · oxidation of 3MC, 4MC, and guaiacol. The two-dimensional drift times vs. m/Q diagrams enable visualization of the number of isomers formed at each m/Q.





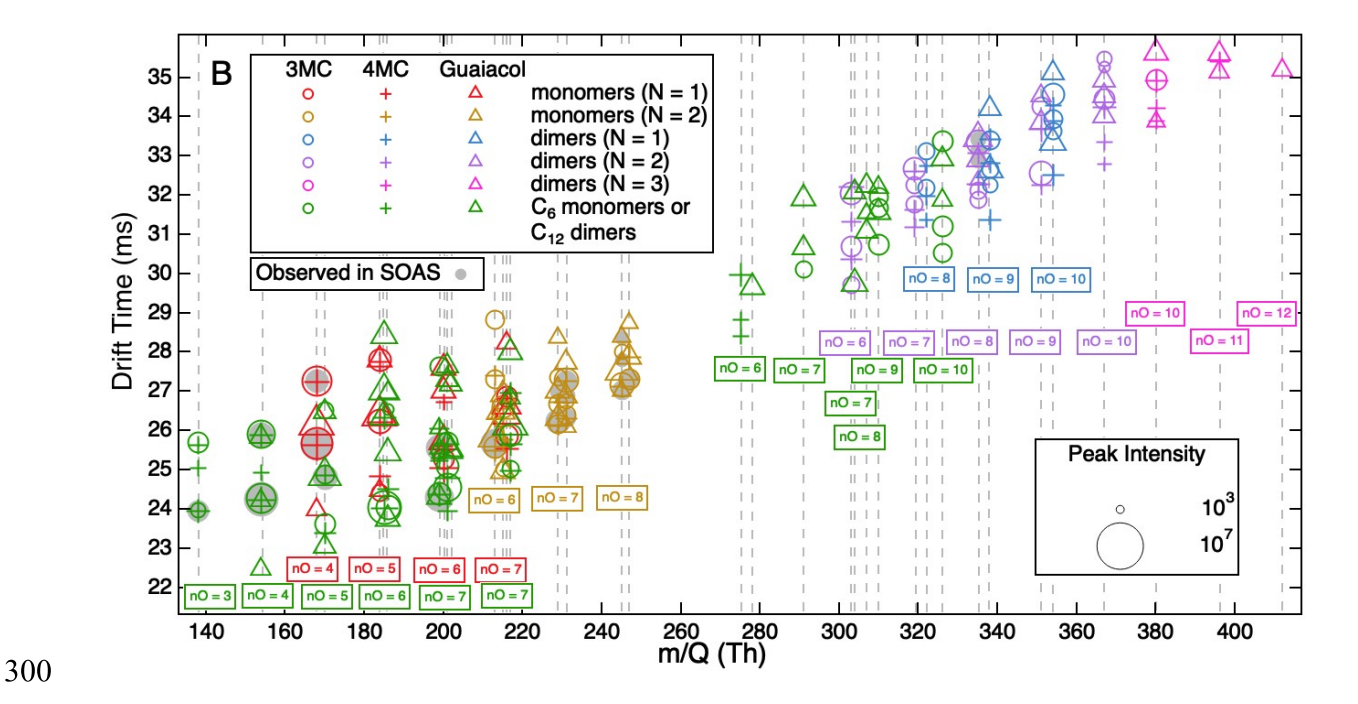


**Figure 4.** (A) 2D drift time vs. m/Q plot for the NO<sub>3</sub>· oxidation experiments of phenol and catechol. (B) 2D drift time vs. m/Q plot for the NO<sub>3</sub>· oxidation experiments of 3MC, 4MC and guaiacol. These products represent monomer and dimer products described in the text. The symbol sizes represent the relative peak intensities in the IMS-TOF. In (A), the drift times of the chemical standards, 2NP, 4NP, and 4NC are labelled. Also shown are the identical compounds identified from the SOAS biomass burning aerosol sample. The vertical dashed lines at the specific m/Qs are for guidance.

## 3.2.1 Formation of nitrophenol products with additional alcohol groups

The chemical formulas of the major SOA products from the five studied phenolic VOCs shown in **Figure 4** are usually featured by the additions of  $xNO_2 + yO - xH$  (x = 1-3, y = 0-3) onto the initial chemical formulas. These formulas could represent addition of  $-NO_2$  groups to the aromatic backbone, forming nitro-phenolic products as widely known. However, the additional oxygens are unexpected for  $NO_3$ · oxidation in which ·OH radicals are predicted to be very low. They could be due to the alcohol groups (-OH) in addition to the  $-NO_2$  groups or formation of  $-NO_3$ · functional groups instead of  $-NO_2$ . It is also unlikely that these products are formed from

peroxy radical cross reactions, as the phenol-derived peroxy radicals (with the  $O_2$ · on an aromatic carbon) do not undergo the Russell mechanism and produce ketones and alcohols as peroxy radicals on aliphatic carbons do (Russell 1957). It is apparent that many identical products (i.e., same m/Q and drift time) are observed in the NO<sub>3</sub>· oxidation of phenol and catechol (**Figure 4A**). These results suggest that although catechol is functionalized with one more alcohol group than phenol, the NO<sub>3</sub>· oxidation of phenol produces a number of identical products, evident for the addition of alcohol groups to the aromatic ring. A representative example for this observation is at m/Q 154 (C<sub>6</sub>H<sub>4</sub>NO<sub>4</sub><sup>-</sup>) in the NO<sub>3</sub>· oxidation of phenol and catechol. Shown in **Figure 5** are the driftgrams for m/Q 154 from the NO<sub>3</sub>· oxidation of (A) phenol, (B) catechol, and (C) the SOAS aerosol sample. Three prominent drift time peaks are present in these samples, at 22.4 ms, 24.2 ms and 25.8 ms. The peak at 24.2 ms was confirmed to be 4NC by the authentic chemical standard. In the NO<sub>3</sub>· oxidation of catechol (**Figure 5B**), only two major drift time peaks were present at m/Q 154, as expected, which would represent 3-nitrocatechol (3NC) and 4NC. This suggests that the peak at 25.8 ms is likely 3NC, but it cannot be definitively assigned due to the lack of a standard for 3NC. With our tentative assignment, the substantial presence of 3NC in the NO<sub>3</sub>· oxidation of catechol is in contrast to previous studies, where only 4NC was detected as a major product (Finewax et al. 2018). One likely explanation is that the presence of  $O_3$  in our study has strongly affected the stability of the intermediate which modifies the products' isomer distribution (Bolzacchini et al. 2001), while the study by Finewax et al., (2018) used N<sub>2</sub>O<sub>5</sub> as the NO<sub>3</sub>· precursor and O<sub>3</sub> was not present. Nonetheless, the perfect drift time peak matching clearly suggests that the NO<sub>3</sub>· oxidation of phenol could produce nitrocatechols. Two possibilities for the additional peak at 22.4 ms are N-nitroresorcinol or N-nitrohydroquinone, which contain their alcohol groups in the 1,3-position and 1,4-positions respectively. Since the alcohol groups are not

317

318

319

320

321

322

323

324

325

326

327

328

329

330

331

332

333

334

335

336

337

338

in the 1,2-positions in these structures, they could only be formed from the NO<sub>3</sub>· oxidation of phenol which is evident at 22.4 ms in **Figure 5A**. We also note that both the nitrocatechol isomers were largely observed from the ambient aerosol sample (**Figure 5C**). These comparisons together suggest that the oxidation of phenolic VOCs produces dynamic and complex isomer distributions, likely mediated by O<sub>3</sub>. Further investigation is warranted to elucidate the mechanistic pathways underlying the formation of 3NC and 4NC from the NO<sub>3</sub>· oxidation of phenol.

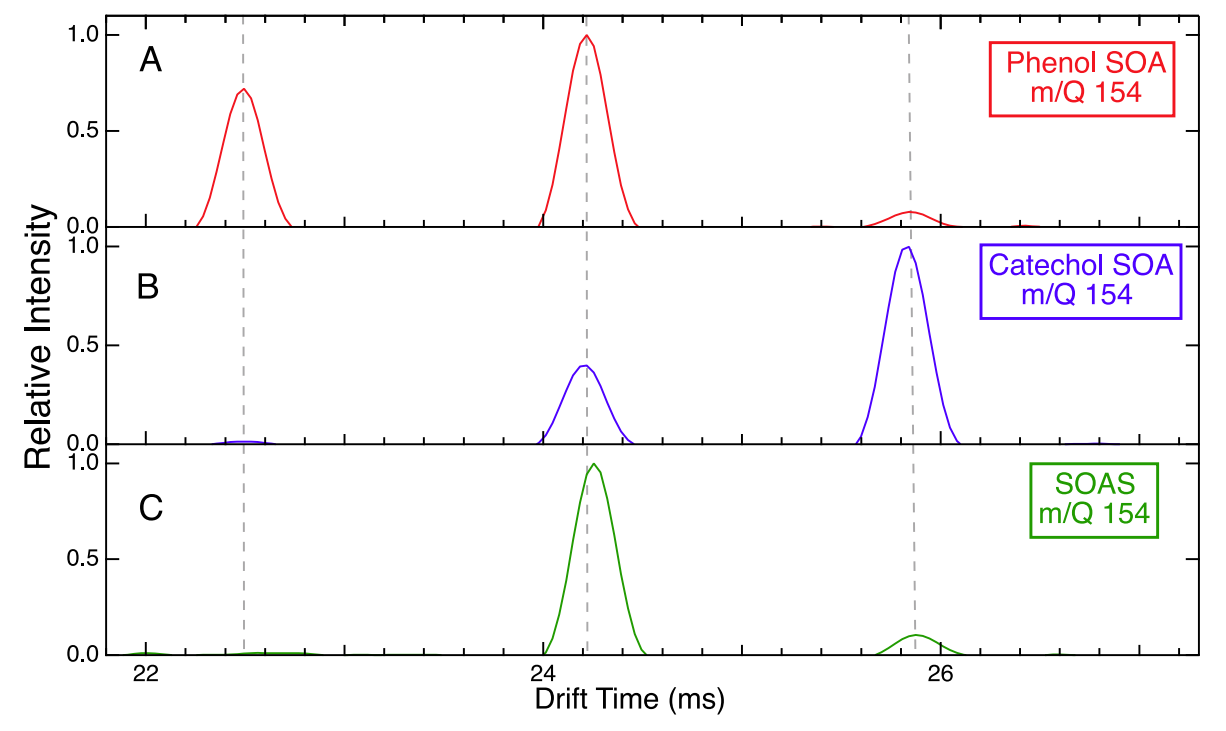


**Figure 5**. Driftgrams of m/Q 154 (C<sub>6</sub>H<sub>4</sub>NO<sub>4</sub><sup>-</sup>) from (A) phenol + NO<sub>3</sub>· SOA, (B) catechol + NO<sub>3</sub>· SOA, and (C) the SOAS aerosol sample.

## 3.2.2 Oxidation products of the C<sub>7</sub> phenolic VOCs

In **Figure 4B**, a number of products with identical chemical formulas were observed in the NO<sub>3</sub>· oxidation of 3MC, 4MC and guaiacol likely because these three phenolic VOCs have the same chemical formula. However, these products are expected to have different structures and thus should be separated by different drift times in the IMS-TOF. This is indeed the case, as evident in

Figure 4B. Regardless, the major monomer products in all three systems appear to be highly consistent with the mechanisms shown in **Figure 3B**. In addition, a variety of six-carbon (C<sub>6</sub>) monomers and twelve-carbon ( $C_{12}$ ) dimers were observed. Many of these products have the same chemical formulas and drift times to the products identified in the NO<sub>3</sub>· oxidation of phenol and catechol, indicating that they may exhibit identical structures. The observation of C<sub>6</sub> phenolic products in the NO<sub>3</sub>· oxidation of the three C<sub>7</sub> substituted phenolic VOCs suggests that the carboncontaining substitutes could be replaced by a -OH or by a -NO<sub>2</sub> group. Despite the fact that a methoxy group (in guaiacol) is typically a much better leaving group than a methyl group (in 3MC and 4MC), the observation of C<sub>6</sub> monomers in the NO<sub>3</sub>· oxidation of 3MC and 4MC implies that some scission mechanism of the substituted groups must have occurred. However, the scope and techniques in the present study did not allow us to propose a mechanism for the observation that requires further studies. Moreover, the presence of C<sub>12</sub> dimers in the NO<sub>3</sub>· oxidation of C<sub>7</sub> phenolic VOCs demonstrate that the C<sub>6</sub> monomers were formed in amounts significant enough to undergo further chemistry including dimerization. The C<sub>14</sub> dimer products, however, have some notable differences than the mechanism shown in Figure 3B. Specifically, dimers with one -NO<sub>2</sub> group are only observed with oxidation number  $(n_0)$  greater than or equal to 8. This observation suggests that simple dimers such as those from a nitromethylcatechol with a methylcatechol ( $n_0 = 6$ ) are not present, in contrast to Figure 3B. This difference is further discussed in Section 3.2.4.

356

357

358

359

360

361

362

363

364

365

366

367

368

369

370

371

372

373

374

375

376

377

378

There are some exceptions where the products share similar drift times between two or all three of these systems in **Figure 4B**. When the drift times of two products from 3MC and 4MC overlap, the only difference between the products is the position of a methyl group which may explain the identical drift times. However, when the products of guaiacol overlap with either 3MC or 4MC, this drift time overlap is not as easily explained because in one case the methyl group is

part of a methoxy group and in the other case, it is attached to the ring. To verify the differences between such "identical" peaks, comparisons were made between the fragmentation mass spectra. For example, similar drift times were observed in the  $NO_3$ · oxidation of 3MC and 4MC at m/Q 168 ( $C_7H_6NO_4$ -) with drift time ~ 25.6 ms, as well as in the  $NO_3$ · oxidation of 3MC, 4MC and guaiacol at m/Q 184 ( $C_7H_6NO_5$ -) with drift time ~ 27.8 ms. **Figures S2** and **S3** compare the fragmentation mass spectra at CID 20V of these products. In both cases, although the peaks have similar drift times in the IMS, it is apparent that the fragmentation mass spectra are distinct, suggesting that they do not have the same chemical structures, as expected. Further research needs to be conducted to explain this observation, but it is possible that the resonance of the aromatic ring largely constrains the CCS of the products and hence the observed drift times.

# 3.2.3 Non-aromatic products

In the analysis of the SOA constituents from NO<sub>3</sub>· oxidation of the phenolic VOCs, products with two additional hydrogens than the above-discussed compounds were observed. These products include: m/Q 185 (C<sub>6</sub>H<sub>5</sub>N<sub>2</sub>O<sub>5</sub>-), and m/Q 201 (C<sub>6</sub>H<sub>5</sub>N<sub>2</sub>O<sub>6</sub>-) in phenol; m/Q 201 (C<sub>6</sub>H<sub>5</sub>N<sub>2</sub>O<sub>6</sub>-) and m/Q 217 (C<sub>6</sub>H<sub>5</sub>N<sub>2</sub>O<sub>7</sub>-) in catechol; and m/Q 215 (C<sub>7</sub>H<sub>7</sub>N<sub>2</sub>O<sub>6</sub>-), m/Q 231 (C<sub>7</sub>H<sub>7</sub>N<sub>2</sub>O<sub>7</sub>-), and m/Q 247 (C<sub>7</sub>H<sub>7</sub>N<sub>2</sub>O<sub>8</sub>-), in 3MC, 4MC and guaiacol oxidation. These peaks were not expected based on the known gas-phase reaction mechanisms (**Figure 3**) but were observed in substantial abundances as shown in **Figure 4**. The addition of two hydrogens in each of these phenolic VOCs effectively reduces the double bond equivalence (DBE) by one and removes its aromaticity or suggests a possible ring-opening. The fragment mass spectra (**Figures S4 – S8**) of these products at CID 20V revealed similar fragmentation patterns across each m/Q for each of the phenolic VOCs studied. In these fragmentation mass spectra, neutral losses of m/Q 31 (HNO), m/Q

47 (HNO<sub>2</sub>), *m/Q* 63 (NO<sub>2</sub> + OH or HNO<sub>3</sub>) are consistently observed to be dominant fragments from the parent compounds. These fragmentation patterns are in contrast to the products with the nitrophenol type of structures (e.g., *m/Q* 213 and *m/Q* 229), which will mainly lose NO<sub>2</sub> (*m/Q* 46) at high CID voltage due to their aromaticity. Unfortunately, the interpretation of these fragments does not help to uncover the exact structures of these products. Thus, it is still unclear how this class of products are produced through NO<sub>3</sub>· oxidation of the phenolic VOCs. Nevertheless, the results suggest that these products are common across different phenolic VOCs and may comprise substantial fractions. It should also be mentioned that despite this loss of aromaticity or possible ring-opening, these products were stable enough to be observed in the presence of NO<sub>3</sub>· and O<sub>3</sub>. This suggests that the products might not contain C=C double bonds which could be quickly oxidized by NO<sub>3</sub>· and O<sub>3</sub>, but rather carbonyls (C=O) on the cyclohexane ring. Further studies are warranted to elucidate the chemical structures and formation mechanisms of these non-aromatic/ring-opening products because such products have not been previously reported in NO<sub>3</sub>· oxidation of the phenolic VOC systems.

### 3.2.4 Dimers in the NO<sub>3</sub>· oxidation products of the phenolic VOCs

All of the phenolic VOCs under study showed the capability to form a wide variety of dimers upon NO<sub>3</sub>· oxidation with up to three nitrogen atoms per dimer molecule. Structural analysis of these dimers was carried out by investigating the mass spectra at the same drift times of the parent ions under high CID 20V. **Figure 6** presents the fragmentation mass spectra of five major dimers in phenol SOA (as shown in the reaction scheme in **Figure 3B**). These dimers are all characterized by the diphenyl ether structures. In the fragmentation mass spectra shown in **Figure 6**, bond scission at the ether linkages are evident, consistent with the proposed structures.

In panels A and B are fragment mass spectra of two single nitro- dimers and both of these show strong peaks indicating the fragmentation of m/Q 92 (phenol). In the case of m/Q 246 in panel B, this loss of phenol indicates that the nitro and alcohol groups are located on the same ring. In panels C and D are fragment mass spectra of two dinitro- dimers and both of these show strong peaks indicating the loss of m/Q 169 (C<sub>6</sub>H<sub>3</sub>NO<sub>5</sub>), possibly suggesting nitrophenol with two alcohol groups as the monomeric building block. Lastly, for m/Q 320, a trinitro-dimer in panel E, a large peak at m/O 138 (nitrophenol) shows the loss of m/O 182 (dinitrophenol). Since there are no additional oxygens in this molecule, the two monomer building blocks can be deduced as nitrophenol and dinitrophenol. Thus, the dimers' monomer building blocks are revealed. From the mechanism shown in Figure 3B, it was assumed that many of the dimers in these systems are formed in the gas phase via phenoxy radical pathways, followed by gas-particle partitioning. This is supported by the observation that volatile building blocks such as phenol and catechol are present in the dimers; they are unlikely to be present in the particle phase in substantial amount and participate in condensed-phase dimerization. Similar gas-phase phenoxy radical chemistry has been proposed previously from both experimental and computational studies (Strollo and Ziemann 2016; Xu et al. 2010). Nevertheless, it is unclear whether all the dimers were formed via this pathway due to the lack of gas-phase measurements. Specifically, the volatile monomeric building blocks were not observed in the C<sub>14</sub> dimers. The simplest single nitro dimer formed in the NO<sub>3</sub>· oxidation of 3MC, 4MC and guaiacol was expected as C<sub>14</sub>H<sub>13</sub>NO<sub>6</sub>, which would be composed of the building blocks C<sub>7</sub>H<sub>8</sub>O<sub>2</sub> and C<sub>7</sub>H<sub>6</sub>NO<sub>4</sub>. However, the smallest single nitro dimer ions observed were C<sub>14</sub>H<sub>12</sub>NO<sub>8</sub> in 3MC and 4MC and C<sub>14</sub>H<sub>12</sub>NO<sub>9</sub> in guaiacol. The reason for such difference is unclear, but the fact that volatile monomer building blocks are not present might indicate that the major C<sub>14</sub> dimers were formed via particle-phase reactions. Regardless, similar types of dimers are

425

426

427

428

429

430

431

432

433

434

435

436

437

438

439

440

441

442

443

444

445

446

observed in all the studied phenolic VOC systems, suggesting that they are important constituents in the phenolic SOA from NO<sub>3</sub>· oxidation.

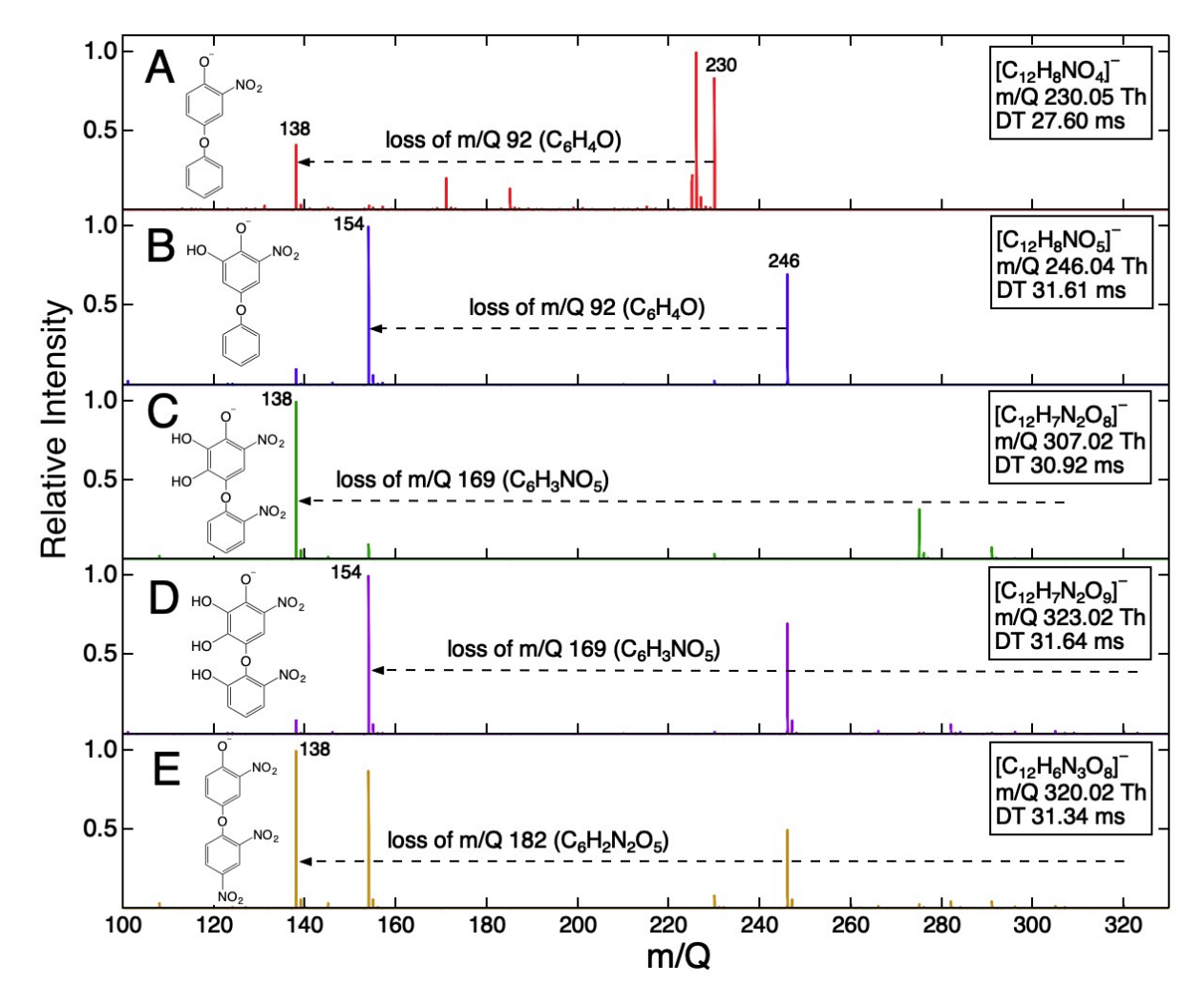


**Figure 6**. Fragment mass spectra of five dimers from the NO<sub>3</sub>· oxidation of phenol performed at CID 20 V with their proposed structures shown on the left. From top to bottom the dimers' formulas are A (C<sub>12</sub>H<sub>8</sub>NO<sub>4</sub>-), B (C<sub>12</sub>H<sub>8</sub>NO<sub>5</sub>-), C (C<sub>12</sub>H<sub>7</sub>N<sub>2</sub>O<sub>8</sub>-), D (C<sub>12</sub>H<sub>7</sub>N<sub>2</sub>O<sub>9</sub>-), E (C<sub>12</sub>H<sub>6</sub>N<sub>3</sub>O<sub>8</sub>-).

## 3.2.5 Phenolic VOC products in ambient biomass burning aerosols

In the analysis of the SOAS aerosol sample, some identical products to those characterized in the NO<sub>3</sub>· oxidation of the five phenolic VOCs in this study were observed and displayed in **Figure 4**. Namely, a variety of C<sub>6</sub> and C<sub>7</sub> monomers as well as several C<sub>14</sub> dimers were identified

in the SOAS biomass burning sample with identical drift times to those observed in our study. Additionally, some products containing additional alcohol groups, such as m/O 170 (C<sub>6</sub>H<sub>4</sub>NO<sub>5</sub>) in phenol and catechol, m/Q 229 ( $C_7H_5N_2O_7$ ) and 245 ( $C_7H_5N_2O_8$ ) in 3MC, 4MC and guaiacol, and non-aromatic compounds, such as m/Q 215 ( $C_7H_7N_2O_6^-$ ), 231 ( $C_7H_7N_2O_7^-$ ) and 247 (C<sub>7</sub>H<sub>7</sub>N<sub>2</sub>O<sub>8</sub>-) in 3MC, 4MC and guaiacol, identified in this study were also present in the SOAS aerosol sample, indicating that these new chemical processes discussed here are relevant to that observed in ambient biomass burning events. Furthermore, we should note that these compounds were only observed in the sample that was collected during a major wildfire event but not in the other 12 non-biomass burning samples, suggesting their relevance to biomass burning aerosol processing. Although it is the only sample relevant to a large biomass burning event at the beginning of the field campaign and its representativeness warrants further examination, the identical products from different pathways are worthwhile to mention. It is also notable that the particular SOAS biomass burning event started before sunrise, but the sample collection was during the morning hours. Therefore, interference from daytime OH-oxidation chemistry and primary emissions cannot be ruled out (Chow et al. 2016; Li et al. 2020b). More distinct ambient aerosol samples with higher time resolution are needed to further confirm how the observed products are formed.

477

478

479

480

481

482

476

460

461

462

463

464

465

466

467

468

469

470

471

472

473

474

475

# 3.3. Optical properties of products from NO<sub>3</sub>· oxidation of phenolic VOCs

The MAC values averaged at the various wavelength ranges for each of the phenolic derivatives are tabulated in **Table 1**. The UV-Vis absorption spectra for each of these compounds can be found in **Figure S9**. The MAC values were calculated for the SOA derived from each phenolic VOC at 365 nm, average of 400 - 550 nm, and average of the entire UV-Vis range (290).

-700 nm). The <MAC>400-500nm values had standard deviations of  $\pm$  0.200 m<sup>2</sup> g<sup>-1</sup> or less. The <MAC $>_{290-700nm}$  values had standard deviations of  $\pm$  1.182 m<sup>2</sup> g<sup>-1</sup> or less. Prior studies have suggested that 365 nm is a characteristic wavelength of peak absorption for BrC (Lin et al. 2014; Zhang et al. 2012c); <MAC><sub>400–550nm</sub> were shown for consistent comparisons with previous measurements (Moise et al. 2015). Among the five studied phenolic VOC systems, guaiacol SOA exhibit somewhat lower light absorption than the other four systems which all absorb light strongly. To our knowledge, this is the first report of optical properties (i.e., MAC values) of phenolic VOC + NO<sub>3</sub>· SOA. Thus, we compared our measurements with laboratory aromatic SOA and ambient organic aerosols relevant to urban atmosphere or biomass burning. Despite that there are some variations between MAC values from different phenolic systems, our results suggest that the measured MAC values from the SOA derived from phenolic VOC + NO<sub>3</sub>· oxidation are generally 3-10 times higher than the laboratory-generated aromatic SOA (e.g., from photooxidation of toluene and the xylenes) (Liu et al. 2015; Nakayama et al. 2013, 2010; Zhong and Jang 2011). These comparisons suggest that the SOA from photooxidation of aromatic VOCs are mostly less absorbing compounds than formed from NO<sub>3</sub>· oxidation in the present work. In addition, prior studies suggest that the guaiacol ·OH oxidation SOA are much more light absorbing when NO<sub>x</sub> was present (i.e.,  $\leq$ MAC $\geq$ <sub>400–550nm</sub> of  $\sim 0.19$  m<sup>2</sup> g<sup>-1</sup> for SOA in the presence of NO<sub>x</sub>; in contrast to that of  $\sim 0.02 - 0.03$  m<sup>2</sup> g<sup>-1</sup> in the absence of NO<sub>x</sub>) (Lambe et al. 2013; Romonosky et al. 2016). Note that the MAC values reported for guaiacol +  $\cdot$ OH/NO<sub>x</sub> are very consistent with our measurements for guaiacol + NO<sub>3</sub>· (i.e., <MAC><sub>400–550nm</sub> of  $\sim$  0.17 m<sup>2</sup> g<sup>-1</sup>). These comparisons could be explained by the fact that both  $\cdot$ OH/NO<sub>x</sub> and NO<sub>3</sub>· oxidation of guaiacol (or other phenolic VOCs) produce substantial nitrophenol-like products (Finewax et al., 2018), but this is not the case for other aromatic VOCs such as toluene and the xylenes, which largely form non-absorbing

483

484

485

486

487

488

489

490

491

492

493

494

495

496

497

498

499

500

501

502

503

504

oxygenated products (Ji et al. 2017; Kamens et al. 2011; Wagner et al. 2003; Zhou et al. 2011). We should also mention that almost all the phenolic SOA constituents observed here contain at least one nitro group on the aromatic rings, which is highly light absorbing. However, when comparing with ambient organic aerosols, especially those relevant to biomass burning events, our results are similar or lower than the ambient OA's MAC values: MAC<sub>365nm</sub> = 1.52 ± 2.10 m<sup>2</sup> g<sup>-1</sup> and <MAC><sub>400-500nm</sub> = 1.76 ± 2.46 m<sup>2</sup> g<sup>-1</sup> (both values are represented as mean ± standard deviation) (Chen and Bond 2010; Cheng et al. 2011; Flowers et al. 2010; Hecobian et al. 2010; Hoffer et al. 2006; Kirchstetter et al. 2004; Lack et al. 2012; Magi 2011, 2009; Utry et al. 2013; Zhang et al. 2013, 2011b). The closer MAC values with ambient organic aerosols imply that nitro- or nitrophenol type of products are substantial, especially from biomass burning aerosols.

# 4. Conclusions and atmospheric implications.

In this work, the SOA constituents from the NO<sub>3</sub>· oxidation of five major phenolic VOCs relevant in ambient biomass burning emissions were analyzed using IMS-TOF. In addition to the nitrophenolic products which have been demonstrated in prior research, our analysis suggested observations of new products indicative of previously unrecognized oxidation mechanisms. These new products and pathways include: (1) formation of multifunctional products containing both – NO<sub>2</sub> and –OH groups; (2) formation of non-aromatic/ring-opening products; (3) formation of diphenyl ether dimers; and (4) formation of fragmentation products when carbon-containing substitutes are present in the phenolic VOCs. These products may form a substantial portion of the total SOA mass. Additionally, the identification of these same products in the SOAS biomass burning sample shows the relevance of these new product pathways in the ambient biomass burning emissions. Although detailed mechanisms that are responsible for these products have not

been elucidated, we suggest that they could be important focuses in future work to improve our understanding of the oxidation and evolution of phenolic VOCs in the atmosphere during nighttime. In particular, how the presence of O<sub>3</sub> influences the isomeric distribution of the oxidation products and how the additional alcohol functional groups are formed are critical to understand as biomass burning is becoming increasingly important globally. Finally, the optical analysis of the SOA from the NO<sub>3</sub>· oxidation of these phenolic VOCs has shown that phenolic VOCs with additional functionalization form products with larger SOA mass and these products tend to absorb light strongly in the UV and visible ranges. This increased functionalization and dimerization both lead to lower SOA volatility and ultimately lead to an increase in light-absorbing brown carbon under atmospheric conditions. The observations reported in this work strengthen the assumption that nighttime NO<sub>3</sub>· oxidation of phenolic VOCs can lead to a significant portion of light-absorbing brown carbon in the atmosphere.

# 541 Declaration of Competing Interest

The authors declare that they have no known competing financial interests or personal

relationships that could have appeared to influence the work reported in this paper.

# Acknowledgements

543

544

545

546

547

548

550

We thank Prof. Paul Ziemann and Zachary Finewax from University of Colorado, Boulder for useful discussions. We thank Prof. Allen Goldstein from University of California, Berkeley for providing the SOAS aerosol samples. The work was supported by the startup funding granted to H.Z. by University of California, Riverside and by the National Science Foundation under Grant

549 AGS-1953905.

#### Credit authorship contribution statement

- Raphael J. Mayorga: Formal Analysis, Investigation, Writing- Original Draft, Data Curation,
- Visualization. Zixu Zhao: Validation. Haofei Zhang: Conceptualization, Methodology,
- 553 Software, Resources, Writing- Review & Editing, Supervision, Project Administration, Funding
- Acquisition.

576

577

578

579

580

581

582

583

584

585

586

587

- Arnold, S.R., Emmons, L.K., Monks, S.A., Law, K.S., Ridley, D.A., Turquety, S., Tilmes, S.,
  Thomas, J.L., Bouarar, I., Flemming, J., Huijnen, V., Mao, J., Duncan, B.N., Steenrod,
  S., Yoshida, Y., Langner, J., Long, Y., 2015. Biomass burning influence on high-latitude
  tropospheric ozone and reactive nitrogen in summer 2008: a multi-model analysis based
  on POLMIP simulations. *Atmospheric Chem. Phys.* **15**, 6047–6068.
  https://doi.org/10.5194/acp-15-6047-2015
- Bloss, C., Wagner, V., Jenkin, M.E., Volkamer, R., Bloss, W.J., Lee, J.D., Heard, D.E., Wirtz, K., Martin-Reviejo, M., Rea, G., Wenger, J.C., Pilling, M.J., 2005. Development of a detailed chemical mechanism (MCMv3.1) for the atmospheric oxidation of aromatic hydrocarbons. *Atmospheric Chem. Phys.* **5**, 641–664. https://doi.org/10.5194/acp-5-641-2005
- Bluvshtein, N., Lin, P., Flores, J.M., Segev, L., Mazar, Y., Tas, E., Snider, G., Weagle, C.,
  Brown, S.S., Laskin, A., Rudich, Y., 2017. Broadband optical properties of biomassburning aerosol and identification of brown carbon chromophores: OPTICAL AND
  CHEMICAL PROPERTIES OF BROWN CARBON AEROSOLS. *J. Geophys. Res.*Atmospheres 122, 5441–5456. https://doi.org/10.1002/2016JD026230
- Bolzacchini, E., Bruschi, M., Hjorth, J., Meinardi, S., Orlandi, M., Rindone, B., Rosenbohm, E.,
   2001. Gas-Phase Reaction of Phenol with NO 3. Environ. Sci. Technol. 35, 1791–1797.
   https://doi.org/10.1021/es001290m
  - Chen, Y., Bond, T.C., 2010. Light absorption by organic carbon from wood combustion. *Atmospheric Chem. Phys.* **10**, 1773–1787. https://doi.org/10.5194/acp-10-1773-2010
  - Cheng, Y., He, K.-B., Zheng, M., Duan, F.-K., Du, Z.-Y., Ma, Y.-L., Tan, J.-H., Yang, F.-M., Liu, J.-M., Zhang, X.-L., Weber, R.J., Bergin, M.H., Russell, A.G., 2011. Mass absorption efficiency of elemental carbon and water-soluble organic carbon in Beijing, China. *Atmospheric Chem. Phys.* 11, 11497–11510. https://doi.org/10.5194/acp-11-11497-2011
  - Chow, K.S., Huang, X.H.H., Yu, J.Z., 2016. Quantification of nitroaromatic compounds in atmospheric fine particulate matter in Hong Kong over 3 years: field measurement evidence for secondary formation derived from biomass burning emissions. *Environ. Chem.* **13**, 665. https://doi.org/10.1071/EN15174
  - Coeur-Tourneur, C., Foulon, V., Laréal, M., 2010. Determination of aerosol yields from 3-methylcatechol and 4-methylcatechol ozonolysis in a simulation chamber. *Atmos. Environ.* **44**, 852–857. https://doi.org/10.1016/j.atmosenv.2009.11.027
- Crutzen, P.J., Andreae, M.O., 1990. Biomass Burning in the Tropics: Impact on Atmospheric
   Chemistry and Biogeochemical Cycles. *Science* 250, 1669–1678.
   https://doi.org/10.1126/science.250.4988.1669
- Fine, P.M., Cass, G.R., Simoneit, B.R.T., 2004. Chemical Characterization of Fine Particle
   Emissions from the Fireplace Combustion of Wood Types Grown in the Midwestern and
   Western United States. *Environ. Eng. Sci.* 21, 387–409.
   https://doi.org/10.1089/109287504323067021
- Finewax, Z., de Gouw, J.A., Ziemann, P.J., 2019. Products and Secondary Organic Aerosol
   Yields from the OH and NO 3 Radical-Initiated Oxidation of Resorcinol. ACS Earth
   Space Chem. 3, 1248–1259. https://doi.org/10.1021/acsearthspacechem.9b00112
- Finewax, Z., de Gouw, J.A., Ziemann, P.J., 2018. Identification and Quantification of 4-Nitrocatechol Formed from OH and NO 3 Radical-Initiated Reactions of Catechol in Air

- in the Presence of NO x: Implications for Secondary Organic Aerosol Formation from
   Biomass Burning. *Environ. Sci. Technol.* 52, 1981–1989.
   https://doi.org/10.1021/acs.est.7b05864
- Fleming, L.T., Lin, P., Roberts, J.M., Selimovic, V., Yokelson, R., Laskin, J., Laskin, A.,
  Nizkorodov, S.A., 2020. Molecular composition and photochemical lifetimes of brown
  carbon chromophores in biomass burning organic aerosol. *Atmospheric Chem. Phys.* **20**,
  1105–1129. https://doi.org/10.5194/acp-20-1105-2020
- Flowers, B.A., Dubey, M.K., Mazzoleni, C., Stone, E.A., Schauer, J.J., Kim, S.-W., Yoon, S.C.,
   2010. Optical-chemical-microphysical relationships and closure studies for mixed
   carbonaceous aerosols observed at Jeju Island; 3-laser photoacoustic spectrometer,
   particle sizing, and filter analysis. *Atmospheric Chem. Phys.* 10, 10387–10398.
   https://doi.org/10.5194/acp-10-10387-2010
- Frka, S., Šala, M., Kroflič, A., Huš, M., Čusak, A., Grgić, I., 2016. Quantum Chemical
   Calculations Resolved Identification of Methylnitrocatechols in Atmospheric Aerosols.
   *Environ. Sci. Technol.* 50, 5526–5535. https://doi.org/10.1021/acs.est.6b00823
- Fry, J.L., Draper, D.C., Barsanti, K.C., Smith, J.N., Ortega, J., Winkler, P.M., Lawler, M.J.,
   Brown, S.S., Edwards, P.M., Cohen, R.C., Lee, L., 2014. Secondary Organic Aerosol
   Formation and Organic Nitrate Yield from NO 3 Oxidation of Biogenic Hydrocarbons.
   Environ. Sci. Technol. 48, 11944–11953. https://doi.org/10.1021/es502204x

- Gao, Y., Chen, S.B., Yu, L.E., 2007. Efflorescence relative humidity of airborne sodium chloride particles: A theoretical investigation. *Atmos. Environ.* **41**, 2019–2023. https://doi.org/10.1016/j.atmosenv.2006.12.014
- Gershenzon, M.Yu., Il'in, Sergeid., Fedotov, N.G., Gershenzon, Y.M., Aparina, E.V., Zelenov, V.V., 1999. The mechanism of reactive NO3 uptake on dry NaX (X=Cl, Br). *J. Atmospheric Chem.* **34**, 119–135. https://doi.org/10.1023/A:1006258205551
- Hatch, L.E., Luo, W., Pankow, J.F., Yokelson, R.J., Stockwell, C.E., Barsanti, K.C., 2015. Identification and quantification of gaseous organic compounds emitted from biomass burning using two-dimensional gas chromatography–time-of-flight mass spectrometry. *Atmospheric Chem. Phys.* **15**, 1865–1899. https://doi.org/10.5194/acp-15-1865-2015
- Hatch, L.E., Yokelson, R.J., Stockwell, C.E., Veres, P.R., Simpson, I.J., Blake, D.R., Orlando, J.J., Barsanti, K.C., 2017. Multi-instrument comparison and compilation of non-methane organic gas emissions from biomass burning and implications for smoke-derived secondary organic aerosol precursors. *Atmospheric Chem. Phys.* 17, 1471–1489. https://doi.org/10.5194/acp-17-1471-2017
- Hecobian, A., Zhang, X., Zheng, M., Frank, N., Edgerton, E.S., Weber, R.J., 2010. Water-Soluble Organic Aerosol material and the light-absorption characteristics of aqueous extracts measured over the Southeastern United States. *Atmospheric Chem. Phys.* **10**, 5965–5977. https://doi.org/10.5194/acp-10-5965-2010
- Hobbs, P.V., 1997. Direct Radiative Forcing by Smoke from Biomass Burning. *Science* 275,
  1777–1778. https://doi.org/10.1126/science.275.5307.1777
- Hoffer, A., Gelencsér, A., Guyon, P., Kiss, G., Schmid, O., Frank, G.P., Artaxo, P., Andreae,
   M.O., 2006. Optical properties of humic-like substances (HULIS) in biomass-burning
   aerosols. Atmospheric Chem. Phys. 6, 3563–3570. https://doi.org/10.5194/acp-6-3563 2006
- Ji, Y., Zhao, J., Terazono, H., Misawa, K., Levitt, N.P., Li, Y., Lin, Y., Peng, J., Wang, Y.,
  Duan, L., Pan, B., Zhang, F., Feng, X., An, T., Marrero-Ortiz, W., Secrest, J., Zhang,

- A.L., Shibuya, K., Molina, M.J., Zhang, R., 2017. Reassessing the atmospheric oxidation mechanism of toluene. *Proc. Natl. Acad. Sci.* **114**, 8169–8174. https://doi.org/10.1073/pnas.1705463114
- Jiang, H., Frie, A.L., Lavi, A., Chen, J.Y., Zhang, H., Bahreini, R., Lin, Y.-H., 2019. Brown
   Carbon Formation from Nighttime Chemistry of Unsaturated Heterocyclic Volatile
   Organic Compounds. *Environ. Sci. Technol. Lett.* 6, 184–190.
   https://doi.org/10.1021/acs.estlett.9b00017
- Kamens, R.M., Zhang, H., Chen, E.H., Zhou, Y., Parikh, H.M., Wilson, R.L., Galloway, K.E.,
  Rosen, E.P., 2011. Secondary organic aerosol formation from toluene in an atmospheric hydrocarbon mixture: Water and particle seed effects. *Atmos. Environ.* **45**, 2324–2334. https://doi.org/10.1016/j.atmosenv.2010.11.007
- Kirchstetter, T.W., Novakov, T., Hobbs, P.V., 2004. Evidence that the spectral dependence of
   light absorption by aerosols is affected by organic carbon: SPECTRAL LIGHT
   ABSORPTION BY AEROSOLS. *J. Geophys. Res. Atmospheres* 109, n/a-n/a.
   https://doi.org/10.1029/2004JD004999
- Kitanovski, Z., Čusak, A., Grgić, I., Claeys, M., 2014. Chemical characterization of the main
   products formed through aqueous-phase photonitration of guaiacol. *Atmospheric Meas*.
   *Tech.* 7, 2457–2470. https://doi.org/10.5194/amt-7-2457-2014
- Kroflič, A., Grilc, M., Grgić, I., 2015. Unraveling Pathways of Guaiacol Nitration in
   Atmospheric Waters: Nitrite, A Source of Reactive Nitronium Ion in the Atmosphere.
   Environ. Sci. Technol. 49, 9150–9158. https://doi.org/10.1021/acs.est.5b01811
- Lack, D.A., Langridge, J.M., Bahreini, R., Cappa, C.D., Middlebrook, A.M., Schwarz, J.P.,
   2012. Brown carbon and internal mixing in biomass burning particles. *Proc. Natl. Acad.* Sci. 109, 14802–14807. https://doi.org/10.1073/pnas.1206575109
- Lambe, A.T., Cappa, C.D., Massoli, P., Onasch, T.B., Forestieri, S.D., Martin, A.T., Cummings,
   M.J., Croasdale, D.R., Brune, W.H., Worsnop, D.R., Davidovits, P., 2013. Relationship
   between Oxidation Level and Optical Properties of Secondary Organic Aerosol. *Environ*.
   Sci. Technol. 47, 6349–6357. https://doi.org/10.1021/es401043j
- Lauraguais, A., Coeur-Tourneur, C., Cassez, A., Deboudt, K., Fourmentin, M., Choël, M., 2014.
  Atmospheric reactivity of hydroxyl radicals with guaiacol (2-methoxyphenol), a biomass burning emitted compound: Secondary organic aerosol formation and gas-phase oxidation products. *Atmos. Environ.* **86**, 155–163.
  https://doi.org/10.1016/j.atmosenv.2013.11.074
- Lauraguais, A., El Zein, A., Coeur, C., Obeid, E., Cassez, A., Rayez, M.-T., Rayez, J.-C., 2016.

  Kinetic Study of the Gas-Phase Reactions of Nitrate Radicals with Methoxyphenol
  Compounds: Experimental and Theoretical Approaches. *J. Phys. Chem. A* 120, 2691–
  2699. https://doi.org/10.1021/acs.jpca.6b02729
- Li, C., He, Q., Hettiyadura, A.P.S., Käfer, U., Shmul, G., Meidan, D., Zimmermann, R., Brown,
   S.S., George, C., Laskin, A., Rudich, Y., 2020a. Formation of Secondary Brown Carbon
   in Biomass Burning Aerosol Proxies through NO 3 Radical Reactions. *Environ. Sci. Technol.* 54, 1395–1405. https://doi.org/10.1021/acs.est.9b05641
- 688 Li, J., Li, J., Wang, G., Zhang, T., Dai, W., Ho, K.F., Wang, Q., Shao, Y., Wu, C., Li, L., 2020b.
  689 Molecular characteristics of organic compositions in fresh and aged biomass burning
  690 aerosols. *Sci. Total Environ.* **741**, 140247.
- https://doi.org/10.1016/j.scitotenv.2020.140247

- Lin, P., Bluvshtein, N., Rudich, Y., Nizkorodov, S.A., Laskin, J., Laskin, A., 2017. Molecular
   Chemistry of Atmospheric Brown Carbon Inferred from a Nationwide Biomass Burning
   Event. *Environ. Sci. Technol.* 51, 11561–11570. https://doi.org/10.1021/acs.est.7b02276
- Lin, P., Fleming, L.T., Nizkorodov, S.A., Laskin, J., Laskin, A., 2018. Comprehensive Molecular
   Characterization of Atmospheric Brown Carbon by High Resolution Mass Spectrometry
   with Electrospray and Atmospheric Pressure Photoionization. *Anal. Chem.* 90, 12493–
   12502. https://doi.org/10.1021/acs.analchem.8b02177
- Lin, P., Liu, J., Shilling, J.E., Kathmann, S.M., Laskin, J., Laskin, A., 2015. Molecular
   characterization of brown carbon (BrC) chromophores in secondary organic aerosol
   generated from photo-oxidation of toluene. *Phys. Chem. Chem. Phys.* 17, 23312–23325.
   https://doi.org/10.1039/C5CP02563J

704

705

706

707

708

709

710

711

712

713

714

- Lin, Y.-H., Budisulistiorini, S.H., Chu, K., Siejack, R.A., Zhang, H., Riva, M., Zhang, Z., Gold, A., Kautzman, K.E., Surratt, J.D., 2014. Light-Absorbing Oligomer Formation in Secondary Organic Aerosol from Reactive Uptake of Isoprene Epoxydiols. *Environ. Sci. Technol.* **48**, 12012–12021. https://doi.org/10.1021/es503142b
  - Liu, P.F., Abdelmalki, N., Hung, H.-M., Wang, Y., Brune, W.H., Martin, S.T., 2015. Ultraviolet and visible complex refractive indices of secondary organic material produced by photooxidation of the aromatic compounds toluene and *m* -xylene. *Atmospheric Chem. Phys.* **15**, 1435–1446. https://doi.org/10.5194/acp-15-1435-2015
- Magi, B.I., 2011. Corrigendum to 'Chemical apportionment of southern African aerosol mass and optical depth' published in Atmos. Chem. Phys., 9, 7643–7655, 2009. *Atmospheric Chem. Phys.* 11, 4777–4778. https://doi.org/10.5194/acp-11-4777-2011
- Magi, B.I., 2009. Chemical apportionment of southern African aerosol mass and optical depth. *Atmospheric Chem. Phys.* **9**, 7643–7655. https://doi.org/10.5194/acp-9-7643-2009
- Matsunaga, A., Ziemann, P.J., 2010. Gas-Wall Partitioning of Organic Compounds in a Teflon
   Film Chamber and Potential Effects on Reaction Product and Aerosol Yield
   Measurements. *Aerosol Sci. Technol.* 44, 881–892.
   https://doi.org/10.1080/02786826.2010.501044
- Moise, T., Flores, J.M., Rudich, Y., 2015. Optical Properties of Secondary Organic Aerosols and
   Their Changes by Chemical Processes. *Chem. Rev.* 115, 4400–4439.
   https://doi.org/10.1021/cr5005259
- Nakao, S., Clark, C., Tang, P., Sato, K., Cocker III, D., 2011. Secondary organic aerosol
   formation from phenolic compounds in the absence of NO x. *Atmospheric Chem. Phys.* 11, 10649–10660. https://doi.org/10.5194/acp-11-10649-2011
- Nakayama, T., Matsumi, Y., Sato, K., Imamura, T., Yamazaki, A., Uchiyama, A., 2010.
   Laboratory studies on optical properties of secondary organic aerosols generated during
   the photooxidation of toluene and the ozonolysis of α -pinene: OPTICAL PROPERTIES
   OF SOAS. *J. Geophys. Res. Atmospheres* 115. https://doi.org/10.1029/2010JD014387
- Nakayama, T., Sato, K., Matsumi, Y., Imamura, T., Yamazaki, A., Uchiyama, A., 2013.

  Wavelength and NO x dependent complex refractive index of SOAs generated from the photooxidation of toluene. *Atmospheric Chem. Phys.* **13**, 531–545.

  https://doi.org/10.5194/acp-13-531-2013
- Olariu, R.I., Bejan, I., Barnes, I., Klotz, B., Becker, K.H., Wirtz, K., 2004. Rate coefficients for the gas-phase reaction of NO3 radicals with selected dihydroxybenzenes. *Int. J. Chem. Kinet.* **36**, 577–583. https://doi.org/10.1002/kin.20029

- Oros, D.R., Simoneit, B.R.T., 2001. Identification and emission factors of molecular tracers in organic aerosols from biomass burning Part 1. Temperate climate conifers. *Appl. Geochem.* **16**, 1513–1544. https://doi.org/10.1016/S0883-2927(01)00021-X
- Pang, H., Zhang, Q., Lu, X., Li, K., Chen, H., Chen, J., Yang, X., Ma, Y., Ma, J., Huang, C.,
   2019. Nitrite-Mediated Photooxidation of Vanillin in the Atmospheric Aqueous Phase.
   Environ. Sci. Technol. 53, 14253–14263. https://doi.org/10.1021/acs.est.9b03649
- Pereira, K.L., Hamilton, J.F., Rickard, A.R., Bloss, W.J., Alam, M.S., Camredon, M., Ward,
   M.W., Wyche, K.P., Muñoz, A., Vera, T., Vázquez, M., Borrás, E., Ródenas, M., 2015.
   Insights into the Formation and Evolution of Individual Compounds in the Particulate
   Phase during Aromatic Photo-Oxidation. *Environ. Sci. Technol.* 49, 13168–13178.
   https://doi.org/10.1021/acs.est.5b03377
- Phillips, G.J., Thieser, J., Tang, M., Sobanski, N., Schuster, G., Fachinger, J., Drewnick, F.,
  Borrmann, S., Bingemer, H., Lelieveld, J., Crowley, J.N., 2016. Estimating
  N<sub&gt;2&lt;/sub&gt;0&lt;sub&gt;5&lt;/sub&gt; uptake coefficients using
  ambient measurements ofNO&lt;sub&gt;3&lt;/sub&gt;
  N&lt;sub&gt;2&lt;/sub&gt;0&lt;sub&gt;5&lt;/sub&gt;
  N&lt;sub&gt;2&lt;/sub&gt;0&lt;sub&gt;
  and particle-phase nitrate. Atmospheric Chem. Phys. 16, 13231–13249.
  https://doi.org/10.5194/acp-16-13231-2016
  - Pope, C.A., Dockery, D.W., 2006. Health Effects of Fine Particulate Air Pollution: Lines that Connect. *J. Air Waste Manag. Assoc.* **56**, 709–742. https://doi.org/10.1080/10473289.2006.10464485

756

757

762

763

764

765

766

767

- Rollins, A.W., Browne, E.C., Min, K.-E., Pusede, S.E., Wooldridge, P.J., Gentner, D.R.,
   Goldstein, A.H., Liu, S., Day, D.A., Russell, L.M., Cohen, R.C., 2012. Evidence for NOx
   Control over Nighttime SOA Formation. *Science* 337, 1210–1212.
   https://doi.org/10.1126/science.1221520
  - Romonosky, D.E., Ali, N.N., Saiduddin, M.N., Wu, M., Lee, H.J. (Julie), Aiona, P.K., Nizkorodov, S.A., 2016. Effective absorption cross sections and photolysis rates of anthropogenic and biogenic secondary organic aerosols. *Atmos. Environ.* **130**, 172–179. https://doi.org/10.1016/j.atmosenv.2015.10.019
  - Russell, G.A., 1957. Deuterium-isotope Effects in the Autoxidation of Aralkyl Hydrocarbons. Mechanism of the Interaction of PEroxy Radicals <sup>1</sup>. *J. Am. Chem. Soc.* **79**, 3871–3877. https://doi.org/10.1021/ja01571a068
- Schwantes, R.H., Schilling, K.A., McVay, R.C., Lignell, H., Coggon, M.M., Zhang, X.,
   Wennberg, P.O., Seinfeld, J.H., 2017. Formation of highly oxygenated low-volatility
   products from cresol oxidation. *Atmospheric Chem. Phys.* 17, 3453–3474.
   https://doi.org/10.5194/acp-17-3453-2017
- Seisel, S., Caloz, F., Fenter, F.F., van den Bergh, H., Rossi, M.J., 1997. The heterogeneous
   reaction of NO 3 with NaCl and KBr: A nonphotolytic source of halogen atoms. *Geophys. Res. Lett.* 24, 2757–2760. https://doi.org/10.1029/97GL02857
- Stewart, D.J., Griffiths, P.T., Cox, R.A., 2004. Reactive uptake coefficients for heterogeneous reaction of N<sub&gt;2&lt;/sub&gt;0&lt;sub&gt;5&lt;/sub&gt; with submicron aerosols of NaCl and natural sea salt. *Atmospheric Chem. Phys.* **4**, 1381–1388. https://doi.org/10.5194/acp-4-1381-2004
- Strollo, C.M., Ziemann, P.J., 2016. Investigation of the formation of benzoyl peroxide, benzoic
   anhydride, and other potential aerosol products from gas—phase reactions of

782 benzoylperoxy radicals. *Atmos. Environ.* **130**, 202–210. https://doi.org/10.1016/j.atmosenv.2016.01.011

- Thornton, J.A., Kercher, J.P., Riedel, T.P., Wagner, N.L., Cozic, J., Holloway, J.S., Dubé, W.P.,
   Wolfe, G.M., Quinn, P.K., Middlebrook, A.M., Alexander, B., Brown, S.S., 2010. A
   large atomic chlorine source inferred from mid-continental reactive nitrogen chemistry.
   Nature 464, 271–274. https://doi.org/10.1038/nature08905
  - Utry, N., Ajtai, T., Filep, Á., Dániel Pintér, M., Hoffer, A., Bozoki, Z., Szabó, G., 2013. Mass specific optical absorption coefficient of HULIS aerosol measured by a four-wavelength photoacoustic spectrometer at NIR, VIS and UV wavelengths. *Atmos. Environ.* **69**, 321–324. https://doi.org/10.1016/j.atmosenv.2013.01.003
  - Vidović, K., Kroflič, A., Šala, M., Grgić, I., 2020. Aqueous-Phase Brown Carbon Formation from Aromatic Precursors under Sunlight Conditions. *Atmosphere* **11**, 131. https://doi.org/10.3390/atmos11020131
    - Vidović, K., Lašič Jurković, D., Šala, M., Kroflič, A., Grgić, I., 2018. Nighttime Aqueous-Phase Formation of Nitrocatechols in the Atmospheric Condensed Phase. *Environ. Sci. Technol.* **52**, 9722–9730. https://doi.org/10.1021/acs.est.8b01161
  - Wagner, V., Jenkin, M.E., Saunders, S.M., Stanton, J., Wirtz, K., Pilling, M.J., 2003. Modelling of the photooxidation of toluene: conceptual ideas for validating detailed mechanisms. *Atmospheric Chem. Phys.* **3**, 89–106. https://doi.org/10.5194/acp-3-89-2003
  - Xu, F., Yu, W., Gao, R., Zhou, Q., Zhang, Q., Wang, W., 2010. Dioxin Formations from the Radical/Radical Cross-Condensation of Phenoxy Radicals with 2-Chlorophenoxy Radicals and 2,4,6-Trichlorophenoxy Radicals. *Environ. Sci. Technol.* **44**, 6745–6751. https://doi.org/10.1021/es101794v
  - Yee, L.D., Kautzman, K.E., Loza, C.L., Schilling, K.A., Coggon, M.M., Chhabra, P.S., Chan, M.N., Chan, A.W.H., Hersey, S.P., Crounse, J.D., Wennberg, P.O., Flagan, R.C., Seinfeld, J.H., 2013. Secondary organic aerosol formation from biomass burning intermediates: phenol and methoxyphenols. *Atmospheric Chem. Phys.* **13**, 8019–8043. https://doi.org/10.5194/acp-13-8019-2013
- Yuan, B., Liggio, J., Wentzell, J., Li, S.-M., Stark, H., Roberts, J.M., Gilman, J., Lerner, B.,
  Warneke, C., Li, R., Leithead, A., Osthoff, H.D., Wild, R., Brown, S.S., de Gouw, J.A.,
  2016. Secondary formation of nitrated phenols: insights from observations during the
  Uintah Basin Winter Ozone Study (UBWOS) 2014. *Atmospheric Chem. Phys.* 16, 2139–
  2153. https://doi.org/10.5194/acp-16-2139-2016
- Zaytsev, A., Koss, A.R., Breitenlechner, M., Krechmer, J.E., Nihill, K.J., Lim, C.Y., Rowe, J.C.,
  Cox, J.L., Moss, J., Roscioli, J.R., Canagaratna, M.R., Worsnop, D.R., Kroll, J.H.,
  Keutsch, F.N., 2019. Mechanistic study of the formation of ring-retaining and ringopening products from the oxidation of aromatic compounds under urban atmospheric
  conditions. *Atmospheric Chem. Phys.* 19, 15117–15129. https://doi.org/10.5194/acp-1915117-2019
- Zhang, H., Lin, Y.-H., Zhang, Z., Zhang, X., Shaw, S.L., Knipping, E.M., Weber, R.J., Gold, A.,
   Kamens, R.M., Surratt, J.D., 2012a. Secondary organic aerosol formation from
   methacrolein photooxidation: roles of NOx level, relative humidity and aerosol acidity.
   *Environ. Chem.* 9, 247. https://doi.org/10.1071/EN12004
- Zhang, H., Surratt, J.D., Lin, Y.H., Bapat, J., Kamens, R.M., 2011a. Effect of relative humidity
   on SOA formation from isoprene/NO photooxidation: enhancement of 2-methylglyceric

- acid and its corresponding oligoesters under dry conditions. *Atmospheric Chem. Phys.* **11**, 6411–6424. https://doi.org/10.5194/acp-11-6411-2011
- Zhang, H., Worton, D.R., Lewandowski, M., Ortega, J., Rubitschun, C.L., Park, J.-H.,
- Kristensen, K., Campuzano-Jost, P., Day, D.A., Jimenez, J.L., Jaoui, M., Offenberg, J.H.,
- Kleindienst, T.E., Gilman, J., Kuster, W.C., de Gouw, J., Park, C., Schade, G.W.,
- Frossard, A.A., Russell, L., Kaser, L., Jud, W., Hansel, A., Cappellin, L., Karl, T.,
- Glasius, M., Guenther, A., Goldstein, A.H., Seinfeld, J.H., Gold, A., Kamens, R.M.,
- Surratt, J.D., 2012b. Organosulfates as Tracers for Secondary Organic Aerosol (SOA)
- Formation from 2-Methyl-3-Buten-2-ol (MBO) in the Atmosphere. *Environ. Sci.*
- 836 *Technol.* **46**, 9437–9446. https://doi.org/10.1021/es301648z
- Zhang, H., Yee, L.D., Lee, B.H., Curtis, M.P., Worton, D.R., Isaacman-VanWertz, G.,
  Offenberg, J.H., Lewandowski, M., Kleindienst, T.E., Beaver, M.R., Holder, A.L.,
- Lonneman, W.A., Docherty, K.S., Jaoui, M., Pye, H.O.T., Hu, W., Day, D.A.,
- Campuzano-Jost, P., Jimenez, J.L., Guo, H., Weber, R.J., de Gouw, J., Koss, A.R.,
- Edgerton, E.S., Brune, W., Mohr, C., Lopez-Hilfiker, F.D., Lutz, A., Kreisberg, N.M.,
- Spielman, S.R., Hering, S.V., Wilson, K.R., Thornton, J.A., Goldstein, A.H., 2018.
- Monoterpenes are the largest source of summertime organic aerosol in the southeastern United States. *Proc. Natl. Acad. Sci.* **115**, 2038–2043.
- https://doi.org/10.1073/pnas.1717513115
- Zhang, X., Lin, Y.-H., Surratt, J.D., Weber, R.J., 2013. Sources, Composition and Absorption Ångström Exponent of Light-absorbing Organic Components in Aerosol Extracts from the Los Angeles Basin. *Environ. Sci. Technol.* **47**, 3685–3693. https://doi.org/10.1021/es305047b
- Zhang, X., Lin, Y.-H., Surratt, J.D., Zotter, P., Prévôt, A.S.H., Weber, R.J., 2011b. Lightabsorbing soluble organic aerosol in Los Angeles and Atlanta: A contrast in secondary organic aerosol: SOLUBLE BROWN CARBON IN LA AND ATLANTA. *Geophys. Res. Lett.* 38, n/a-n/a. https://doi.org/10.1029/2011GL049385
- Zhang, X., Liu, Z., Hecobian, A., Zheng, M., Frank, N.H., Edgerton, E.S., Weber, R.J., 2012c.
   Spatial and seasonal variations of fine particle water-soluble organic carbon (WSOC)
   over the southeastern United States: implications for secondary organic aerosol
   formation. *Atmospheric Chem. Phys.* 12, 6593–6607. https://doi.org/10.5194/acp-12-6593-2012
- Zhang, X., Zhang, H., Xu, W., Wu, X., Tyndall, G.S., Orlando, J.J., Jayne, J.T., Worsnop, D.R., Canagaratna, M.R., 2019. Molecular characterization of alkyl nitrates in atmospheric aerosols by ion mobility mass spectrometry. *Atmospheric Meas. Tech.* **12**, 5535–5545. https://doi.org/10.5194/amt-12-5535-2019
- Zhao, Z., Le, C., Xu, Q., Peng, W., Jiang, H., Lin, Y.-H., Cocker, D.R., Zhang, H., 2019a.
   Compositional Evolution of Secondary Organic Aerosol as Temperature and Relative
   Humidity Cycle in Atmospherically Relevant Ranges. *ACS Earth Space Chem.* 3, 2549–2558. https://doi.org/10.1021/acsearthspacechem.9b00232
- Zhao, Z., Tolentino, R., Lee, J., Vuong, A., Yang, X., Zhang, H., 2019b. Interfacial Dimerization
   by Organic Radical Reactions during Heterogeneous Oxidative Aging of Oxygenated
   Organic Aerosols. J. Phys. Chem. A 123, 10782–10792.
- 870 https://doi.org/10.1021/acs.jpca.9b10779

871	Zhao, Z., Yang, X., Lee, J., Tolentino, R., Mayorga, R., Zhang, W., Zhang, H., 2020. Diverse
872	Reactions in Highly Functionalized Organic Aerosols during Thermal Desorption. ACS
873	Earth Space Chem. 4, 283–296. https://doi.org/10.1021/acsearthspacechem.9b00312
874	Zhong, M., Jang, M., 2011. Light absorption coefficient measurement of SOA using a UV-
875	Visible spectrometer connected with an integrating sphere. Atmos. Environ. 45, 4263–
876	4271. https://doi.org/10.1016/j.atmosenv.2011.04.082
877	Zhou, Y., Zhang, H., Parikh, H.M., Chen, E.H., Rattanavaraha, W., Rosen, E.P., Wang, W.,
878	Kamens, R.M., 2011. Secondary organic aerosol formation from xylenes and mixtures of
879	toluene and xylenes in an atmospheric urban hydrocarbon mixture: Water and particle
880	seed effects (II). Atmos. Environ. 45, 3882–3890.
881	https://doi.org/10.1016/j.atmosenv.2010.12.048
882	